

Synthetic Thermal and RGB Videos for Automatic Pain Assessment utilizing a Vision-MLP Architecture

Stefanos Gkikas[†]

Department of Electrical & Computer Engineering
Hellenic Mediterranean University
Heraklion, Greece
gkikas@ics.forth.gr

Manolis Tsiknakis[‡]

Department of Electrical & Computer Engineering
Hellenic Mediterranean University
Heraklion, Greece
tsiknaki@ics.forth.gr

Abstract—Pain assessment is essential in developing optimal pain management protocols to alleviate suffering and prevent functional decline in patients. Consequently, reliable and accurate automatic pain assessment systems are essential for continuous and effective patient monitoring. This study presents synthetic thermal videos generated by *Generative Adversarial Networks* integrated into the pain recognition pipeline and evaluates their efficacy. A framework consisting of a *Vision-MLP* and a *Transformer*-based module is utilized, employing RGB and synthetic thermal videos in unimodal and multimodal settings. Experiments conducted on facial videos from the *BioVid* database demonstrate the effectiveness of synthetic thermal videos and underline the potential advantages of it.

Index Terms—Pain recognition, deep learning, GANs, transformers, multi-task learning, data fusion

I. INTRODUCTION

Pain, as defined by the International Association for the Study of Pain (IASP), is “*an unpleasant sensory and emotional experience associated with actual or potential tissue damage, or described in terms of such damage*” [1]. Additionally, Williams and Craig [2] state that pain encompasses emotional, cognitive, and social dimensions beyond physical aspects. Biologically, pain is a distasteful sensation that originates in the peripheral nervous system. It serves a vital function by activating sensory neurons, alerting the body to potential injury, and playing a critical role in recognizing and reacting to hazards. [3]. Pain is a significant concern impacting individuals and social structures. Daily, people across all age groups suffer from pain resulting from accidents, illnesses, or as a part of medical treatment, making it the most common cause for seeking medical consultation. Both acute and chronic pain present clinical, economic, and social challenges. In addition to its immediate impact on a patient’s life, pain is related to several adverse outcomes, including opioid consumption, drug misuse, addiction, deteriorating social relationships, and mental health issues [4]. Effective pain assessment is crucial for early diagnosis, disease advancement monitoring, and treatment effectiveness, particularly in chronic pain management [5]. Consequently, pain is referred to as “*the fifth vital sign*” in nursing literature [6]. Objective measurement of pain is vital for

providing appropriate care, especially for groups who cannot express their pain, such as infants, young children, people with mental health issues, and seniors. Numerous methods are utilized for pain assessment, including self-reporting, which remains the gold standard for determining pain presence and intensity through rating scales and questionnaires. Additionally, behavioral indicators such as facial expressions, vocalizations, and body movements are essential for evaluating pain. [7]. Furthermore, physiological indicators such as electrocardiography, electromyography, skin conductance, and breathing rates provide significant insights into pain’s physical effects [5]. Although pain evaluation holds significant importance, it poses a substantial challenge to medical practitioners [8], particularly with patients who cannot communicate verbally. In senior patients, the situation becomes even more complex due to their decreased expressiveness or reluctance to share their pain experiences [9]. Furthermore, extensive studies [10]–[12] reveal distinct disparities in pain expression among various genders and age categories, underlining the intricacy of the pain assessment process.

In recent years, there has been a growing tendency in the field of affective computing research to incorporate thermal imaging techniques [13]. The interest was sparked following findings in the literature that stress and cognitive load significantly impact skin temperature [14]. This is due to the role of the autonomic nervous system (ANS) in controlling physiological signals like heart rate, respiration rate, blood perfusion, and body temperature, which are indicative of human emotions and affects [13]. Additionally, muscle contractions influence facial temperature by transferring heat to the facial skin [15]. Therefore, thermal imaging is a promising method for measuring transient facial temperatures [16]. The authors in [17] examined thermal imaging and facial action units to assess emotions, including frustration, boredom, and enjoyment. The multimodal approach demonstrated the highest accuracy. Thermal imaging has been explored in a relatively small number of studies within the field of pain research. In [18], the authors observed that facial temperature rises following a painful stimulus, indicating that thermal cameras could serve as valuable tools for pain monitoring. In [19], a pain dataset comprising RGB, thermal, and depth videos was introduced. The findings demonstrated that the RGB modality marginally

[†]: Corresponding Author, [‡]: Affiliated Researcher at the Computational Biomedicine Laboratory of the Foundation for Research and Technology (FORTH), Heraklion, Greece

surpassed the others in performance while integrating all modalities led to superior results.

This study introduces the generation of synthetic thermal videos through generative adversarial networks (GANs), which are used in unimodal and multimodal settings combined with the RGB video modality. The foundation of the automatic pain assessment pipeline is a framework that integrates a Vision Multilayer Perceptron (MLP) model with a transformer-based module. The primary contributions of our research include: (1) generating synthetic thermal videos to supplement pain assessment as an additional vision modality, (2) evaluating the effectiveness of RGB and synthetic thermal videos as independent modalities, (3) exploring the effectiveness of the thermal-related information, and (4) analyzing the performance and application of the newly introduced Vision-MLP architectures.

II. RELATED WORK

Recent developments have seen a range of innovative methods to assess pain levels from video data. Werner *et al.* [20] focused on domain-specific features, using facial action markers with a deep random forest (RF) classifier, and proposed a 3D distance computation method among facial points while in [21], an optical flow method was introduced to track facial points and capture expression changes across frames. The dynamic aspects of pain were addressed by developing long short-term memory networks combined with sparse coding (SLSTM) [22]. Tavakolian *et al.* [23] utilized 3D convolutional neural networks (CNNs) with varied temporal depths to analyze short-, mid-, and long-term facial expressions. In [24], the authors leverage the temporal aspect of videos by encoding frames into motion history and optical flow images, which were then analyzed using a combination of CNN and bidirectional LSTM (biLSTM). Another method encoded videos into single RGB images through statistical spatiotemporal distillation (SSD) and trained a Siamese network in a self-supervised manner [25]. In [26] the authors implemented a multi-stream CNN for feature extraction from different facial regions, applying learned weights to emphasize the significance of each region's features in expressing pain. Further research [27] identified that specific frames more clearly displayed pain expressions and developed a framework using CNNs, gated recurrent units (GRUs), and attention saliency maps, assigning weights to each frame's influence on overall pain intensity. A novel approach by Huang *et al.* [28] was introduced by extracting simulated heart rate data from video content utilizing a 3D CNN, demonstrating strong results in binary and multiclass classification scenarios. Finally, in the studies [29], [30], transformer-based frameworks were proposed, yielding promising results with high efficiency.

III. METHODOLOGY

This section describes the process of generating synthetic thermal videos, the architecture of the proposed automatic pain assessment framework, the developed augmentation techniques, the pre-processing methods, and the pre-training strategy for the modules.

A. Synthetic Thermal Videos

An image-to-image translation (I2I) approach has been developed for generating synthetic thermal videos. I2I generative models aim to map distinct image domains by learning the intrinsic data distributions of both domains. In this case, the source domain consists of RGB images, while thermal images represent the target domain. In this study, conditional generative adversarial networks (cGANs) [31] were developed and trained in supervised settings with aligned image pairs. Fig. 1 illustrates a high-level overview of the proposed method. The generator G generates realistic-looking images, while discriminator D aims to distinguish authentic images from synthetic ones via the following minimax game:

$$\min_G \max_D \mathcal{L}_{\text{cGAN}}(G, D), \quad (1)$$

where the objective function $\mathcal{L}_{\text{cGAN}}(G, D)$ can be expressed as:

$$\mathbb{E}_{x,y}[\log D(x, y)] + \mathbb{E}_{x,z}[\log(1 - D(x, G(x, z)))], \quad (2)$$

where x represents the real data, y signifies the target data, and z denotes the random noise vector. The G aims to minimize the objective function, while the D functions adversarially, trying to maximize it. Furthermore, we included the Wasserstein gradient penalty (WGAN-GP) [32] to increase the training stability. The final objective is described as:

$$\mathcal{L}_{\text{cGAN}}(G, D) + \lambda \mathbb{E}_{\hat{x}, y}[(\|\nabla_{\hat{x}} D(\hat{x}, y)\|_2 - 1)^2], \quad (3)$$

where λ denotes the penalty coefficient. Regarding the architecture, in the proposed methodology, inspired by [33], the G is structured into 3 distinct modules: an encoder, which comprises 2 convolutional layers downsampling the input; an intermediate ResNet module, consisting of 9 residual blocks, each consisting with 2 convolutional layers; and a decoder, upsampling the feature maps to the final resolution (*i.e.*, 256×256) for the synthetic sample. The D founded on [34] is a pixel-level PatchGAN discriminator using 1×1 kernels consisting of 2 convolutional layers.

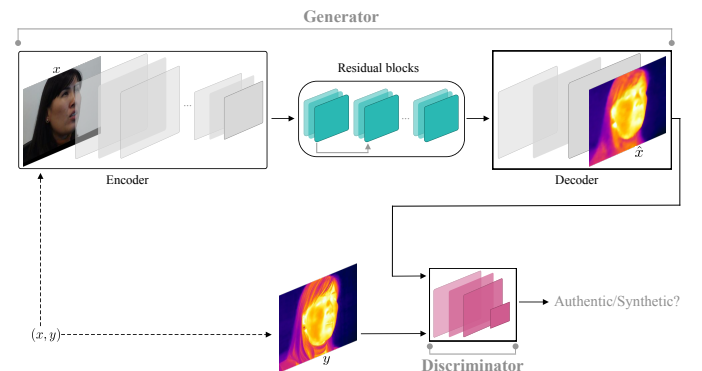


Fig. 1: Overview of the pipeline for generating synthetic thermal images, including the Generator G (Encoder, intermediate ResNet, Decoder), and the Discriminator D .

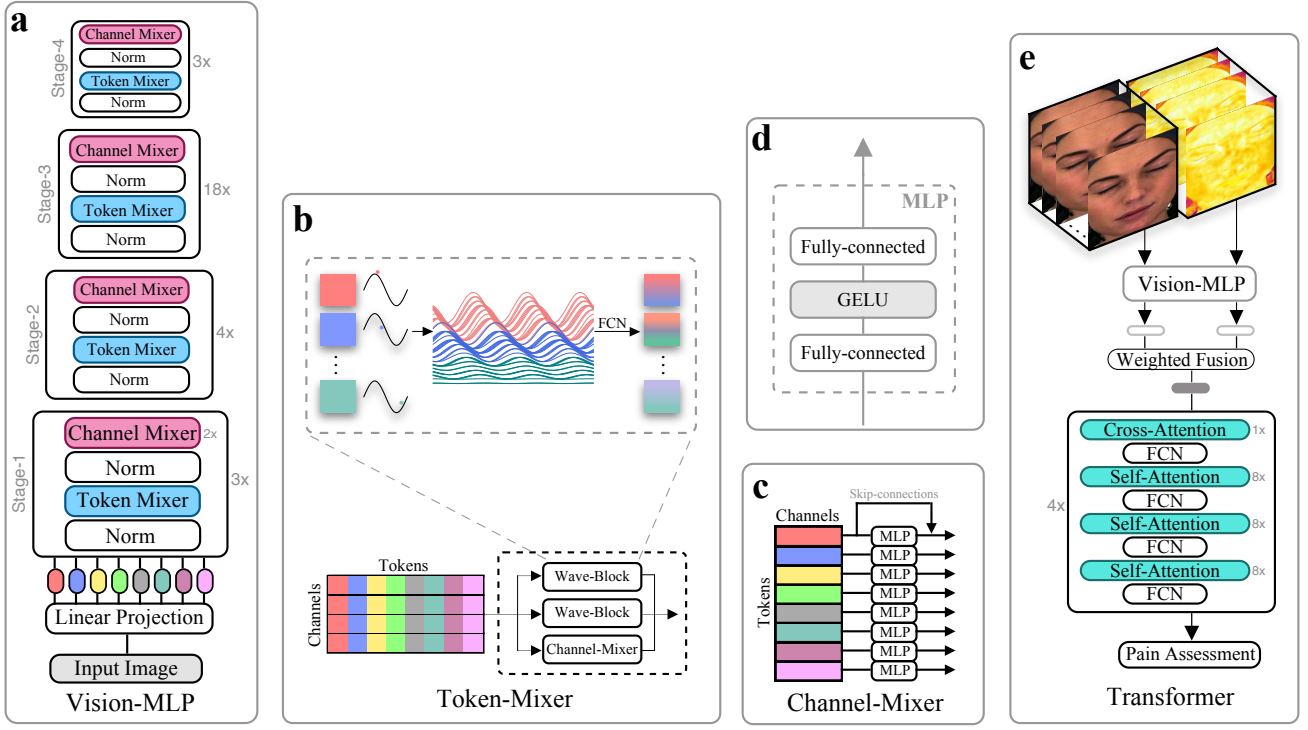


Fig. 2: Schematic overview of the proposed framework for automatic pain assessment, detailing its modules and their primary components: **(a)** The *Vision-MLP* module, responsible for extracting embeddings from individual frames. **(b)** The *Token-Mixer*, another major sub-module of *Vision-MLP*, creates the wave representation for the tokens. **(c)** The *Channel-Mixer*, a key sub-module within *Vision-MLP*. **(e)** The fusion process combining RGB and synthetic thermal embeddings, followed by the *Transformer* module, which performs the final pain assessment.

B. Framework Architecture

The proposed framework comprises two main modules: a *Vision-MLP* model that functions as a spatial embedding extractor for individual video frames and a transformer-based model that serves as a temporal module, utilizing the embedded representations of the videos for temporal analysis and final pain assessment. Fig. 2 illustrates the modules and their primary building blocks.

1) *Vision-MLP*: MLP-like models represent a newly introduced type of vision models, serving as alternatives to traditional Convolutional Neural Networks (CNNs) and Vision Transformers (ViT). They are characterized by simple architectures consisting of fully connected layers coupled with activation functions. They embody lesser inductive bias and are based on basic matrix multiplication routines. Our approach is founded on the principles of [35] introducing the *Vision-MLP* and [36] incorporating a wave representation for the patches (also referred to as tokens). Each video frame is initially divided into n non-overlapping tokens $\mathcal{F}_m = [f_{m,1}, f_{m,2}, \dots, f_{m,n}] \in \mathbb{R}^{n \times p \times p \times 3}$, where p specifies the resolution of each token, *i.e.*, 16×16 pixels, and 3 represents the number of color channels. Each token is then linearly projected into a dimension $d = 768$ before being fed into the *Vision-MLP* (refer to Fig. 2a). The first main sub-module is the so-called *Channel-Mixer* (Fig. 2c), which operates on each token f_j independently and allows

communication between different channels and is formulated as:

$$\text{Channel-Mixer}(f_j, W^c) = W^c f_j \quad (4)$$

where W^c denotes the weight matrix with learnable parameters, and $j = 1, 2, \dots, n$. Next, the second main sub-module, *Token-Mixer* (Fig. 2b), allows communication between different tokens, enabling feature extraction from different spatial locations. Typically, in MLP-based models, the token-mixers formulated as:

$$\text{Token-Mixer}(\mathcal{F}, W^t)_j = \sum_k W_{jk}^t \odot f_k, \quad (5)$$

where W^t denotes the corresponding weight matrix for the tokens, and the \odot represents element-wise multiplication. Our proposed approach transforms the tokens into wave-like representations to modulate the relationship between tokens and weights dynamically according to their semantic content. In order to represent a token f_j as wave \tilde{f}_j through a wave function, amplitude and phase information are needed:

$$\tilde{f}_j = |f_j| \odot e^{i\theta_j}. \quad (6)$$

Here, i denotes the imaginary unit satisfying $i^2 = -1$. The term $|f_j|$ represents the amplitude of the signal. The function $e^{i\theta_j}$ is a periodic function, and θ_j symbolizes the phase of the signal. The amplitude $|f_j|$ can be likened to the real-valued feature

found in conventional models, with the notable distinction being the application of the absolute value operation. In the practical implementation, the absolute value operation is omitted and replaced with 4 for simplicity. The phase θ_j for each token reflects its position within a wave’s cycle and can thus be described using fixed parameters, which are learnable during the training phase. Consequently, 4 is also utilized for the phase estimation. Given that 6 characterizes a wave within the complex domain, the Euler formula facilitates embedding tokens within the neural network architecture:

$$\tilde{f}_j = |f_j| \odot \cos \theta_j + i |f_j| \odot \sin \theta_j. \quad (7)$$

Combining 5 and 7, a token is represented as:

$$f_j = \sum W_{jk}^t f_k \odot \cos \theta_k + W_{jk}^i f_k \odot \sin \theta_k \quad (8)$$

$$\implies \sum W_{jk}^t f_k \odot \cos(W^c f_k) + W_{jk}^i f_k \odot \sin(W^c f_k) \quad (9)$$

where W^t , W^c and W^i are learnable weight matrices. The process described, which pertains to wave-like representations, unfolds within the *Token-Mixer*, particularly in the *Wave-Block*. The *Token-Mixer* architecture comprises three blocks: two *Wave-Blocks* and one *Channel-Mixer* operating in parallel. The *Vision-MLP* module is structured into four stages. Each stage comprises a sequence consisting of a *Token-Mixer* and a *Channel-Mixer* block, with a normalization layer preceding each. The depth of parallel blocks in each stage is 3, 4, 18, and 3, respectively. This structure facilitates extracting hierarchical embeddings with corresponding dimensions across stages 64, 128, 320, and 100.

2) *Fusion*: For each input frame, the *Vision-MLP* extracts an embedding with a dimensionality of $d = 100$. Subsequently, the embeddings derived from the respective frames of a particular video are concatenated to create a unified embedding representation of the original video:

$$\mathcal{V}_D = [d_1 \| d_2 \| \dots \| d_m], \quad \mathcal{V}_D \in \mathbb{R}^N, \quad (10)$$

where m denotes the number of frames in a video, and N represents the dimensionality of the final embedding. Subsequently, the embeddings derived from RGB and synthetic thermal videos are integrated through a weighted fusion process:

$$\mathcal{V}_{Fused} = w_1 \cdot \mathcal{V}_{RGB} + w_2 \cdot \mathcal{V}_{Thermal}, \quad \mathcal{V}_{Fused} \in \mathbb{R}^N. \quad (11)$$

The fusion process is founded on combining the corresponding embeddings, utilizing learned weights w_1 and w_2 , which modulate the contributions of the RGB and thermal embeddings, respectively. The weighted addition provides an optimized integration, reflecting the importance of each modality in the final fused representation \mathcal{V}_{Fused} .

3) *Transformer*: The fused embeddings are subsequently fed into a transformer-based module comprising self-attention and cross-attention blocks (Fig. 2e). The self-attention process is represented as follows:

$$Attention(Q, K, V) = softmax \left(\frac{QK^T}{\sqrt{d_k}} V \right). \quad (12)$$

Here, $Q \in \mathbb{R}^{M \times C}$, $K \in \mathbb{R}^{M \times C}$, and $V \in \mathbb{R}^{M \times C}$ represent the Query, Key, and Value matrices, respectively, where M denotes the input dimension, and C the channel dimension. Similarly, the cross-attention mechanism employs a dot product operation, but the Q instead of $M \times C$ is $N \times C$, where $N < M$ offers a computational cost reduction. Each self and cross-attention block incorporates 1 and 8 attention heads, respectively, while 4 parallel blocks comprise the whole *Transformer* module. The resulting output embeddings, with a dimensionality of 340, are employed to complete the final pain assessment through a fully connected neural network.

C. Augmentation Methods

Two augmentation techniques have been implemented within the framework. First, the so-called *Basic* is employed, integrating polarity inversion with noise addition. This method transforms the original input embedding by reversing the polarity of data elements and adding random noise from a Gaussian distribution, creating variability and perturbations. Second, the *Masking* involves applying zero-valued masks to the embeddings, nullifying segments of the vectors. The dimensions of the masks are randomly determined, spanning 10% to 50% of the embedding’s total dimensions, and they are positioned at random locations within the embeddings.

D. Pre-processing

The pre-processing involved face detection to isolate the facial region. The MTCNN face detector [37] was employed, which utilizes multitask cascaded convolutional neural networks for predicting faces and landmarks. It is important to note that the face detector was applied only to the individual RGB frames, and the coordinates of the detected face were applied to the corresponding synthetic thermal frames. The resolution of all frames was set at 224×224 pixels.

E. Pre-training

For the I2I approach, the *SpeakingFaces* [38] dataset was utilized to train the proposed GAN model for translating the RGB to synthetic thermal videos. In addition, prior to the automatic pain assessment training process, the *Vision-MLP* and *Transformer* modules were pre-trained. The *Vision-MLP* underwent a three-stage pre-training strategy: initially, it was trained on *DigiFace-1M* [39] to learn basic facial features. Subsequently, it was trained on *AffectNet* [40] and *RAF Face Database basic* [41] to learn features related to basic emotions through multi-task learning. Finally, the *Compound Facial Expressions of Emotions Database* [42] and the *RAF Face Database compound* [41] were utilized to learn features of compound emotions in a similar multi-task setting. The multi-task learning process is described as:

$$L_{total} = [e^{w_1} L_{S_1} + w_1] + [e^{w_2} L_{S_2} + w_2], \quad (13)$$

where L_S is the loss for the corresponding task related to different datasets, and w represents the learned weights that drive the learning process in minimizing the combined loss L_{total} , considering all the individual losses. The *Transformer*

TABLE I: Datasets utilized for the pretraining process of the framework.

Dataset	# samples	# classes	Task
<i>SpeakingFaces</i> [38]	4.58M	142	Face [⊗]
<i>DigiFace-1M</i> [39]	1.00M	10,000	Face [⊗]
<i>AffectNet</i> [40]	0.40M	8	Emotion [⊗]
<i>Compound FEE-DB</i> [42]	6,000	26	Emotion [⊗]
<i>RAF-DB basic</i> [41]	15,000	7	Emotion [⊗]
<i>RAF-DB compound</i> [41]	4,000	11	Emotion [⊗]

⊗: includes face image pairs for the I2I task ⊕: includes images for face or emotion recognition tasks

TABLE II: Training details for automatic pain assessment, number of parameters and FLOPS of each module.

Training Details	Vision-MLP	Transformer
Optimizer: <i>AdamW</i>	Params: 7.35 M	Params: 7.96 M
Learning rate: $2e-5$	FLOPS: 30.95 G	FLOPS: 30.90 G
LR decay: <i>cosine</i>		
Weight decay: 0.1		
Warmup epochs: 5		
Batch size: 32		
Total	Params: 15.31 Millions	FLOPS: 61.85 Giga

was pre-trained only on the *DigiFace-1M* [39], where the input images were flattened into 1D vectors due to its architectural design. Table I details the datasets used in the pre-training procedure.

IV. EXPERIMENTAL EVALUATION & RESULTS

The *BioVid Heat Pain Database* [43], was utilized to evaluate the proposed framework. It comprises facial videos, electrocardiogram, electromyogram, and skin conductance levels from 87 healthy individuals. The experimental design of the dataset utilized a thermode to induce pain in the participants’ right arm, resulting in five distinct intensity levels: no pain (NP), mild pain (P_1), moderate pain (P_2), severe pain (P_3), and very severe pain (P_4). Each participant was exposed to each level of pain intensity 20 times, resulting in 100 data samples for each modality and 1740 data samples per class. We utilized the videos ($5 \times 1740 = 8700$) from Part A of *BioVid* in this study. The pain assessment experiments were structured in binary and multi-level classification settings, evaluating each modality individually and in combination. In binary classification, the task was to distinguish between No Pain (NP) and very severe pain (P_4). In contrast, multi-level classification (MC) involves classifying all pain levels within the dataset. For evaluation, the leave-one-subject-out (LOSO) cross-validation method was adopted, and performance was assessed based on the accuracy metric. Table II presents the framework’s training details related to the automatic pain assessment task, and outlines the number of parameters and the computational cost in terms of floating-point operations (FLOPS) for each module.

TABLE III: Classification results utilizing the RGB video modality, reported on accuracy %.

Epochs	Augmentations			Task	
	<i>Basic</i>	<i>Masking</i>	P(Aug)	NP vs P_4	MC
200	✓	10-20	0.7	69.37	30.23
200	✓	20-50	0.7	70.26	28.50
300	✓	30-50	0.9	70.05	30.02

Masking: indicates the percentage of the input embedding to which zero-value masking is applied P(Aug): represents the probability of applying the augmentation methods of Basic & Masking NP: No Pain P_4 : Very Severe Pain MC: multiclass pain level

TABLE IV: Classification results utilizing the synthetic thermal video modality, reported on accuracy %.

Epochs	Augmentations			Task	
	<i>Basic</i>	<i>Masking</i>	P(Aug)	NP vs P_4	MC
200	✓	10-20	0.7	69.97	30.04
200	✓	20-50	0.7	70.20	30.50
300	✓	30-50	0.9	70.69	29.60

A. RGB Videos

In the RGB video modality context, we observed an accuracy of 69.37% for the binary classification task (NP vs. P_4) and 30.23% for the multi-class classification (MC). Upon intensifying the *Masking* augmentation method to encompass 20 – 50% of the input embeddings, there was a modest improvement of 0.89% in accuracy for the binary task. In contrast, a decrement was observed in the multi-class task. Subsequent extension of training to 300 epochs, 30 – 50% for the *Masking* method and 90% probability for both the augmentation methods yielded accuracies of 70.05% and 30.02% for the binary and multi-class tasks, respectively, translating to an average increment marginally below 0.5%. Table III presents the classification results.

B. Synthetic Thermal Videos

In the experiments conducted with the synthetic thermal modality under identical experimental conditions, initial accuracies were recorded at 69.97% for the binary task and 30.04% for the multi-class task. An increase in the intensity of the masking method resulted in modest accuracy improvements of 0.23% and 0.46% for the binary and multi-class tasks, respectively. Subsequently, final accuracy measurements were 70.69% for the binary task and 29.60% for the multi-class task, culminating in an average increase of 0.28%. This difference may arise from the challenge of discerning subtle facial changes associated with low-level pain and accompaniment by further corruption from heavier augmentation, which results in diminished performances. The corresponding results are summarized in Table IV.

C. Additional Analysis on RGB & Synthetic Thermal Videos

The findings from IV-A and IV-B revealed a notable circumstance where the performance metrics for the RGB and synthetic thermal modalities are remarkably similar. Specifically, the highest recorded accuracies for the RGB modality were 70.26% and 30.23% for the NP vs. P4 and MC tasks, respectively. Correspondingly, the peak accuracies for the synthetic thermal modality were 70.69% and 30.50%. On average, the performances from the thermal videos are approximately 1% superior to those of the RGB modality. This outcome was unexpected, given that the synthetic modality was initially presumed to be less effective than the original. This prompted an exploration into the reason synthetic modalities exhibit comparable or superior performance to the original RGB modality. A primary question was regarding the richness and effectiveness of the thermal-related information incorporated in the synthetic videos. The hypothesis suggested that reducing facial expressions in the thermal videos could allow a more explicit assessment of the thermal information. Gaussian blurring was progressively applied to RGB and synthetic thermal videos (refer to Fig. 3), with kernel sizes k incrementally adjusted from 0 to 191. Similar, albeit less time-intensive, experiments to IV-A, IV-B were conducted.

Table V shows that with a kernel size of $k = 0$, the performance disparity of 0.47% (favoring the thermal modality) aligns with prior experimental outcomes. As blurring intensifies to $k = 41$, this discrepancy marginally increases to 0.49%. Notably, at $k = 91$, the divergence expands to 2.13% and intensifies to 5.90% when the blur peaks at $k = 191$ (heavily blurred). The classification performances demonstrated that by diminishing the visibility of facial expressions through blurring, the synthetic thermal videos resulted in superior performance compared to the RGB, with figures of 66.24% over 60.34%. Additionally, as the kernel size increased from $k = 0$ to $k = 191$, the decline in accuracy rates for the synthetic thermal and RGB modalities was 1.81% and 7.13%, respectively. This suggests that the residual information in the synthetic modality, essentially the visually represented facial temperature, remains intact or minimally influenced. Fig. 4 depicts the embedding distribution for the RGB and synthetic thermal modality for $k = 0$ and $k = 191$. Although the separation of the data points is not clear, we observe a distinct difference in the distribution. For $k = 191$, the RGB embeddings are centralized and probably overlap, and a plethora of points are notably spread away from the central mass without a clear pattern. Respectively, the data points are much more uniformly spreading for the synthetic modality, suggesting potentially better differentiation between classes.

D. Fusion

Three fusion methods were assessed in the context of multimodal analysis for RGB and synthetic thermal videos. The approach outlined in 11 was initially applied, utilizing learned weights w_1 and w_2 to scale the respective modalities. Additionally, a second method was employed where a third weight, w_3 , was introduced, resulting in $w_3 \cdot (w_1 \cdot \mathcal{V}_{RGB} + w_2 \cdot \mathcal{V}_{Thermal})$.



Fig. 3: Progressive blurring of RGB and synthetic thermal facial imagery: a sequence illustrating varying degrees of Gaussian blur applied, with kernel sizes incrementally adjusted from $k = 0$ (clear) to $k = 191$ (heavily blurred).

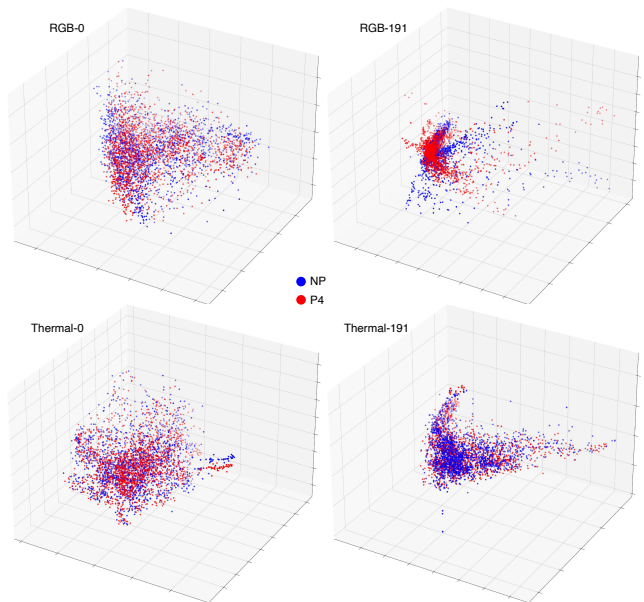


Fig. 4: 3D embedding space distributions of NP (no pain) and P4 (very severe pain) classes in RGB and synthetic thermal videos, for $k = 0$ (clear) and $k = 191$ (heavily blurred).

TABLE V: Classification results utilizing the RGB & the synthetic thermal video modality reported, on accuracy %.

Epochs	Modality	Blur	Augmentations			Task
			Basic	Masking	P(Aug)	NP vs P4
100	RGB	0	✓	10-20	0.7	67.47
100	Thermal	0	✓	10-20	0.7	68.05
100	RGB	41	✓	10-20	0.7	66.61
100	Thermal	41	✓	10-20	0.7	67.10
100	RGB	91	✓	10-20	0.7	64.80
100	Thermal	91	✓	10-20	0.7	66.93
100	RGB	191	✓	10-20	0.7	60.34
100	Thermal	191	✓	10-20	0.7	66.24

Blur: Gaussian blurring with kernel sizes k

TABLE VI: Classification results utilizing the fusion of RGB & synthetic thermal video modality, reported on accuracy %.

Epochs	Fusion weights	Augmentations			Task	
		<i>Basic</i>	<i>Masking</i>	P(Aug)	NP vs P ₄	MC
100	–	✓	10-20	0.7	64.92	26.40
100	W2	✓	10-20	0.7	65.08	26.50
100	W3	✓	10-20	0.7	64.42	25.90
300	W2	✓	10-20	0.7	69.50	29.80
500	W2	✓	10-20	0.7	71.03	30.70

W2: utilization of $[w_1, w_2]$ W3: utilization of $[w_1, w_2, w_3]$

Lastly, a method without learned weights was explored, directly adding the embedding vectors from both modalities. Table VI presents the corresponding results. The absence of weights resulted in 64.92% and 26.40% accuracy for the binary and multi-class tasks, respectively. The integration of the three weights resulted in a decrease of 0.5% in accuracy for both tasks, whereas the application of weights w_1 and w_2 yielded the highest performance, with accuracies reaching 65.08% and 26.50% for the binary and multi-class tasks, respectively. By applying weights w_1 and w_2 and increasing the training period from 100 to 300 epochs while maintaining consistent augmentation settings, accuracies of 69.50% and 29.80% were achieved for the binary and multi-class tasks, respectively. Further extending the training time to 500 epochs without encountering any overfitting phenomena improved performance, reaching accuracies of 71.03% and 30.70% for the respective tasks.

V. COMPARISON WITH EXISTING METHODS

This section compares the proposed method with other existing approaches in the literature. The evaluation utilizes Part A of the *BioVid* dataset, involving all 87 subjects, and follows the same validation protocol, LOSO cross-validation. Table VII presents the corresponding results. The proposed vision-based method, utilizing RGB and synthetic thermal modalities, demonstrated performances comparable to or exceeding that of previous methods. Compared to the findings reported in studies [21], [22], [24], [25], improved accuracy was attained in binary and multi-level tasks. It is noted that the authors in [20] reported accuracies of 72.40% and 30.80%, showing an improvement of 1.37% and 0.10% over our results. In the study [29], the authors achieved the highest reported results, employing a transformer-based architecture.

Furthermore, in Table VIII, we compare our findings with those from the study [19], in which the authors introduce the *MIntPAIN* dataset, including both RGB and thermal videos for automatic pain assessment across five intensity levels. We observe that the accuracy of the RGB and thermal modalities is particularly similar, at 18.55% and 18.33%, respectively. This outcome mirrors our findings, where performance between the two modalities—RGB and synthetic thermal was similarly aligned. By fusing the modalities, the authors achieved an

TABLE VII: Comparison of studies that utilized *BioVid*, videos, and LOSO cross-validation, reported on accuracy%.

Study	Method	Task	
		NP vs P ₄	MC
Werner <i>et al.</i> [20]	Deep RF	72.40	30.80
Werner <i>et al.</i> [21]	RF	70.20	–
Zhi <i>et al.</i> [22]	SLSTM	61.70	29.70
Thiam <i>et al.</i> [24]	2D CNN, biLSTM	69.25	–
Tavakolian <i>et al.</i> [25]	2D CNN	71.00	–
Gkikas <i>et al.</i> [29]	Vision-Transformer	73.28	31.52
Our	Vision-MLP	71.03	30.70

TABLE VIII: Comparison with the *MIntPAIN* dataset, reported on accuracy%.

Study	Dataset	Modality	Task
			MC
Haque <i>et al.</i> [19]	MIntPAIN	RGB	18.55
		Thermal ^o	18.33
		Fusion	30.77
Our	BioVid	RGB	30.02
		Thermal*	29.69
		Fusion	30.70

^o:real ^{*}: synthetic

increase of 30.77%, marking an improvement of over 12%. This contrasts with our results, where the increase was marginal. However, it is important to note that the performances of the unimodal approaches in [19] were below the guess prediction threshold of 20%, and only through the fusion of these modalities did the performance surpass it.

VI. CONCLUSION

This study explored the generation of synthetic thermal imagery from GAN models to evaluate its effectiveness in the context of automatic pain assessment. Furthermore, a novel framework based on *Vision-MLP* was introduced, complimented by a *Transformer* module serving as the core of the assessment system. The conducted experiments underscored the efficacy of the synthetic thermal modality, showcasing performances comparable to or surpassing those of the original RGB modality. Moreover, this study examined the underlying factors contributing to this effectiveness, particularly focusing on the role of temperature color representations. Additionally, the integration of the two vision modalities was analyzed using various fusion techniques. It should be emphasized that further optimization and experimentation, particularly with the multimodal approach, have the capacity to yield enhanced results. We believe that the generation and integration of synthetic modalities, such as thermal imagery, in an automatic pain assessment framework holds significant potential, and additional exploration and research are needed.

ETHICAL IMPACT STATEMENT

This research employed the *BioVid Heat Pain Database* [43] to evaluate the proposed methods. The data were recorded according to the ethical guidelines of Helsinki (*ethics committee: 196/10-UBB/bal*). Prior to commencing data collection, each participant's pain threshold (where sensation transitions from heat to pain) and tolerance threshold (the moment when pain becomes unbearable) were determined. The facial images presented in this study are from participants who have consented to their use for illustrative purposes within a scientific research context. This study aims to introduce a pain assessment framework designed to facilitate continuous patient monitoring while reducing human biases. However, it is essential to recognize that real-world applications, especially in clinical settings, might present challenges, necessitating further experimentation and comprehensive evaluation through clinical trials before deployment.

In addition, this study utilized the *SpeakingFaces* [38] dataset for the image-to-image translation process. The data was collected according to the ethical guidelines of the Declaration of Helsinki, and with the approval from the Institutional Research Ethics Committee at Nazarbayev University. All participants were volunteers who were fully informed about the data collection procedures and the intended use of identifiable images, which will be distributed as part of a dataset. Each participant provided their permission by signing informed consent forms.

Furthermore, several datasets were utilized to pretrain the proposed pain assessment framework. The *DigiFace-1M* [39] is a synthetic dataset where 511 initial face scans were obtained with consent and employed to build a parametric face geometry and texture library model. All the identities and samples were generated from these source data. The *AffectNet* [40] dataset is compiled using search engine queries. The original paper does not explicitly detail ethical compliance measures such as adherence to the Declaration of Helsinki or informed consent procedures. The original paper of *Compound FEE-DB* [42] does not mention ethical compliance measures, but only that the subjects were recruited from the Ohio State University area and received a monetary reward for participating. The *RAF-DB* [41] dataset was compiled using the Flickr image hosting service. Although Flickr hosts both public and privately shared images, the authors do not explicitly mention the type of the downloaded images.

ACKNOWLEDGEMENT

Research supported by the *ODIN* project that has received funding from the European Union's Horizon 2020 research and innovation program under grant agreement No 101017331.

REFERENCES

- [1] S. N. Raja, D. B. Carr, M. Cohen, N. B. Finnerup, H. Flor, S. Gibson, F. J. Keefe, J. S. Mogil, M. Ringkamp, K. A. Sluka, X.-J. Song, B. Stevens, M. D. Sullivan, P. R. Tutelman, T. Ushida, and K. Vader, "The revised international association for the study of pain definition of pain: concepts, challenges, and compromises," *Pain*, vol. 161, no. 9, p. 1976–1982, September 2020.
- [2] A. C. d. C. Williams and K. D. Craig, "Updating the definition of pain," *Pain*, vol. 157, no. 11, pp. 2420–2423, nov 2016.
- [3] K. S and T. RS, "Neuroanatomy and neuropsychology of pain," *Cureus*, vol. 9, no. 10, oct 2017.
- [4] P. Dinakar and A. M. Stillman, "Pathogenesis of pain," *Seminars in Pediatric Neurology*, vol. 23, no. 3, pp. 201–208, aug 2016.
- [5] S. Gkikas and M. Tsiknakis, "Automatic assessment of pain based on deep learning methods: A systematic review," *Computer Methods and Programs in Biomedicine*, vol. 231, p. 107365, 2023.
- [6] L. A. Joel, "The fifth vital sign: pain," *AJN The American Journal of Nursing*, vol. 99, no. 2, p. 9, 1999.
- [7] R. Fernandez Rojas, N. Brown, G. Waddington, and R. Goecke, "A systematic review of neurophysiological sensing for the assessment of acute pain," *NPJ Digital Medicine*, vol. 6, no. 1, p. 76, 2023.
- [8] S. A. H. Aqajari, R. Cao, E. Kasaeyan Naeini, M.-D. Calderon, K. Zheng, N. Dutt, P. Liljeborg, S. Salanterä, A. M. Nelson, and A. M. Rahmani, "Pain assessment tool with electrodermal activity for postoperative patients: method validation study," *JMIR mHealth and uHealth*, vol. 9, no. 5, p. e25258, 2021.
- [9] H. H. Yong, S. J. Gibson, D. J. Horne, and R. D. Helme, "Development of a pain attitudes questionnaire to assess stoicism and cautiousness for possible age differences," *The journals of gerontology. Series B, Psychological sciences and social sciences*, vol. 56, no. 5, pp. P279–84, sep 2001.
- [10] E. J. Bartley and R. B. Fillingim, "Sex differences in pain: a brief review of clinical and experimental findings," *British journal of anaesthesia*, vol. 111, no. 1, pp. 52–58, jul 2013.
- [11] S. Gkikas, C. Chatzaki, E. Pavlidou, F. Verigou, K. Kalkanis, and M. Tsiknakis, "Automatic pain intensity estimation based on electrocardiogram and demographic factors," *SciTePress*, 2022, pp. 155–162.
- [12] S. Gkikas, C. Chatzaki, and M. Tsiknakis, "Multi-task neural networks for pain intensity estimation using electrocardiogram and demographic factors," in *Information and Communication Technologies for Ageing Well and e-Health*. Springer Nature Switzerland, 2023, pp. 324–337.
- [13] M. M. Al Qudah, A. S. Mohamed, and S. L. Lutfi, "Affective state recognition using thermal-based imaging: A survey," *Computer Systems Science & Engineering*, vol. 37, no. 1, 2021.
- [14] S. Ioannou, V. Gallese, and A. Merla, "Thermal infrared imaging in psychophysiology: Potentialities and limits," *Psychophysiology*, vol. 51, no. 10, pp. 951–963, 2014.
- [15] S. Jarlier, D. Grandjean, S. Delplanque, K. N'Diaye, I. Cayeux, M. I. Velazco, D. Sander, P. Vuilleumier, and K. R. Scherer, "Thermal analysis of facial muscles contractions," *IEEE Transactions on Affective Computing*, vol. 2, no. 1, pp. 2–9, 2011.
- [16] A. Merla, L. Di Donato, P. Rossini, and G. Romani, "Emotion detection through functional infrared imaging: preliminary results," *Biomedizinische Technik*, vol. 48, no. 2, pp. 284–286, 2004.
- [17] Y. Mohamed, A. Güneysu, S. Lemaignan, and I. Leite, "Multi-modal affect detection using thermal and optical imaging in a gamified robotic exercise," *International Journal of Social Robotics*, Oct 2023.
- [18] V. K. Erel and H. S. Özkan, "Thermal camera as a pain monitor," *Journal of Pain Research*, vol. 10, pp. 2827–2832, 2017.
- [19] M. A. Haque, R. B. Bautista, F. Noroozi, K. Kulkarni, C. B. Laursen, R. Irani, M. Bellantonio, S. Escalera, G. Anbarjafari, K. Nasrollahi, O. K. Andersen, E. G. Spaich, and T. B. Moeslund, "Deep multimodal pain recognition: A database and comparison of spatio-temporal visual modalities," in *2018 13th IEEE International Conference on Automatic Face & Gesture Recognition (FG 2018)*, 2018, pp. 250–257.
- [20] P. Werner, A. Al-Hamadi, K. Limbrecht-Ecklundt, S. Walter, S. Gruss, and H. C. Traue, "Automatic pain assessment with facial activity descriptors," *IEEE Transactions on Affective Computing*, vol. 8, no. 3, pp. 286–299, 2016.
- [21] P. Werner, A. Al-Hamadi, and S. Walter, "Analysis of facial expressiveness during experimentally induced heat pain," in *2017 Seventh International Conference on Affective Computing and Intelligent Interaction Workshops and Demos (ACIIW)*, 2017, pp. 176–180.
- [22] R. Zhi and M. Wan, "Dynamic facial expression feature learning based on sparse rnn," in *Proceedings of 2019 IEEE 8th Joint International Information Technology and Artificial Intelligence Conference, ITAIC 2019*. Institute of Electrical and Electronics Engineers Inc., may 2019, pp. 1373–1377.
- [23] M. Tavakolian and A. Hadid, "A spatiotemporal convolutional neural network for automatic pain intensity estimation from facial dynamics,"

International Journal of Computer Vision, vol. 127, no. 10, pp. 1413–1425, oct 2019.

- [24] P. Thiam, H. A. Kestler, and F. Schwenker, “Two-stream attention network for pain recognition from video sequences,” *Sensors (Switzerland)*, vol. 20, no. 3, p. 839, feb 2020.
- [25] M. Tavakolian, M. Bordallo Lopez, and L. Liu, “Self-supervised pain intensity estimation from facial videos via statistical spatiotemporal distillation,” *Pattern Recognition Letters*, vol. 140, pp. 26–33, 2020.
- [26] D. Huang, Z. Xia, L. Li, K. Wang, and X. Feng, “Pain-awareness multistream convolutional neural network for pain estimation,” *Journal of Electronic Imaging*, vol. 28, no. 04, p. 1, 2019.
- [27] D. Huang, Z. Xia, J. Mwesigye, and X. Feng, “Pain-attentive network: a deep spatio-temporal attention model for pain estimation,” *Multimedia Tools and Applications*, vol. 79, no. 37-38, pp. 28 329–28 354, 2020.
- [28] D. Huang, X. Feng, H. Zhang, Z. Yu, J. Peng, G. Zhao, and Z. Xia, “Spatio-temporal pain estimation network with measuring pseudo heart rate gain,” *IEEE Transactions on Multimedia*, vol. 24, pp. 3300–3313, 2022.
- [29] S. Gkikas and M. Tsiknakis, “A full transformer-based framework for automatic pain estimation using videos,” in *2023 45th Annual International Conference of the IEEE Engineering in Medicine & Biology Society (EMBC)*, 2023, pp. 1–6.
- [30] S. Gkikas, N. S. Tachos, S. Andreadis, V. C. Pezoulas, D. Zaridis, G. Gkoiis, A. Matonaki, T. G. Stavropoulos, and D. I. Fotiadis, “Multimodal automatic assessment of acute pain through facial videos and heart rate signals utilizing transformer-based architectures,” *Frontiers in Pain Research*, vol. 5, 2024.
- [31] M. Mirza and S. Osindero, “Conditional generative adversarial nets,” *arXiv preprint arXiv:1411.1784*, 2014.
- [32] I. Gulrajani, F. Ahmed, M. Arjovsky, V. Dumoulin, and A. C. Courville, “Improved training of wasserstein gans,” in *Advances in Neural Information Processing Systems*, I. Guyon, U. V. Luxburg, S. Bengio, H. Wallach, R. Fergus, S. Vishwanathan, and R. Garnett, Eds., vol. 30. Curran Associates, Inc., 2017.
- [33] T.-C. Wang, M.-Y. Liu, J.-Y. Zhu, A. Tao, J. Kautz, and B. Catanzaro, “High-resolution image synthesis and semantic manipulation with conditional gans,” in *Proceedings of the IEEE Conference on Computer Vision and Pattern Recognition (CVPR)*, June 2018.
- [34] P. Isola, J.-Y. Zhu, T. Zhou, and A. A. Efros, “Image-to-image translation with conditional adversarial networks,” in *Proceedings of the IEEE conference on computer vision and pattern recognition*, 2017, pp. 1125–1134.
- [35] I. O. Tolstikhin, N. Houlsby, A. Kolesnikov, L. Beyer, X. Zhai, T. Unterthiner, J. Yung, A. Steiner, D. Keysers, J. Uszkoreit, M. Lucic, and A. Dosovitskiy, “Mlp-mixer: An all-mlp architecture for vision,” in *Advances in Neural Information Processing Systems*, M. Ranzato, A. Beygelzimer, Y. Dauphin, P. Liang, and J. W. Vaughan, Eds., vol. 34. Curran Associates, Inc., 2021, pp. 24 261–24 272.
- [36] Y. Tang, K. Han, J. Guo, C. Xu, Y. Li, C. Xu, and Y. Wang, “An image patch is a wave: Phase-aware vision mlp,” in *2022 IEEE/CVF Conference on Computer Vision and Pattern Recognition (CVPR)*, 2022, pp. 10925–10934.
- [37] K. Zhang, Z. Zhang, Z. Li, and Y. Qiao, “Joint face detection and alignment using multitask cascaded convolutional networks,” *IEEE signal processing letters*, vol. 23, no. 10, pp. 1499–1503, 2016.
- [38] M. Abdrakhmanova, A. Kuzdeuov, S. Jarju, Y. Khassanov, M. Lewis, and H. A. Varol, “Speakingfaces: A large-scale multimodal dataset of voice commands with visual and thermal video streams,” *Sensors*, vol. 21, no. 10, 2021.
- [39] G. Bae, M. de La Gorce, T. Baltrušaitis, C. Hewitt, D. Chen, J. Valentin, R. Cipolla, and J. Shen, “Digiface-1m: 1 million digital face images for face recognition,” in *Proceedings of the IEEE/CVF Winter Conference on Applications of Computer Vision (WACV)*, January 2023, pp. 3526–3535.
- [40] A. Mollahosseini, B. Hasani, and M. H. Mahoor, “Affectnet: A database for facial expression, valence, and arousal computing in the wild,” *IEEE Transactions on Affective Computing*, vol. 10, no. 1, pp. 18–31, 2019.
- [41] S. Li, W. Deng, and J. Du, “Reliable crowdsourcing and deep locality-preserving learning for expression recognition in the wild,” in *Proceedings of the IEEE Conference on Computer Vision and Pattern Recognition (CVPR)*, July 2017.
- [42] S. Du, Y. Tao, and A. M. Martinez, “Compound facial expressions of emotion,” *Proceedings of the National Academy of Sciences*, vol. 111, no. 15, pp. E1454–E1462, 2014.
- [43] S. Walter, S. Gruss, H. Ehleiter, J. Tan, H. C. Traue, S. Crawcour, P. Werner, A. Al-Hamadi, A. O. Andrade, and G. M. D. Silva, “The biovid heat pain database: Data for the advancement and systematic validation of an automated pain recognition,” 2013, pp. 128–131.

APPENDIX

Supplementary Metrics

TABLE IX: Classification results utilizing the RGB video modality, reported on recall and F1 score.

Epochs	Augmentations			Metric	Task	
	Basic	Masking	P(Aug)		NP vs P ₄	MC
200	✓	30-50	0.9	Recall	71.29	29.61
				F1	68.53	27.22
200	✓	30-50	0.9	Recall	71.93	24.43
				F1	69.61	23.78
300	✓	30-50	0.9	Recall	71.34	30.64
				F1	69.65	26.12

TABLE X: Classification results utilizing the synthetic thermal video modality, reported on recall and F1 score.

Epochs	Augmentations			Metric	Task	
	Basic	Masking	P(Aug)		NP vs P ₄	MC
200	✓	30-50	0.9	Recall	72.04	28.80
				F1	69.16	26.45
200	✓	30-50	0.9	Recall	72.18	30.89
				F1	69.44	26.45
300	✓	30-50	0.9	Recall	72.52	24.96
				F1	70.01	23.43

TABLE XI: Classification results utilizing the fusion of RGB & synthetic thermal video modality, reported on recall and F1 score.

Epochs	Fusion weights	Augmentations			Metric	Task	
		Basic	Masking	P(Aug)		NP vs P ₄	MC
100	–	✓	30-50	0.9	Recall	67.05	21.68
					F1	62.96	18.29
100	W2	✓	30-50	0.9	Recall	68.72	21.69
					F1	62.98	19.35
100	W3	✓	30-50	0.9	Recall	66.12	23.12
					F1	59.72	19.67
300	W2	✓	30-50	0.9	Recall	71.40	26.39
					F1	68.82	26.18
500	W2	✓	10-20	0.7	Recall	73.20	29.69
					F1	70.30	27.84